High-speed superresolution imaging of the proteins in fission yeast clathrin-mediated endocytic actin patches

Rajesh Arasada[a], Wasim A. Sayyad[a], Julien Berro[b,c,d], and Thomas D. Pollard[a,b,c,*]
[a]Departments of Molecular Cellular and Developmental Biology, [b]Departments of Molecular Biophysics and Biochemistry, [c]Department of Cell Biology, and [d]Nanobiology Institute, Yale University, New Haven, CT 06520-8103

ABSTRACT **To internalize nutrients and cell surface receptors via clathrin-mediated endocytosis, cells assemble at least 50 proteins, including clathrin, clathrin-interacting proteins, actin filaments, and actin binding proteins, in a highly ordered and regulated manner. The molecular mechanism by which actin filament polymerization deforms the cell membrane is unknown, largely due to lack of knowledge about the organization of the regulatory proteins and actin filaments. We used high-speed superresolution localization microscopy of live fission yeast cells to improve the spatial resolution to ~35 nm with 1-s temporal resolution. The nucleation promoting factors Wsp1p (WASp) and Myo1p (myosin-I) define two independent pathways that recruit Arp2/3 complex, which assembles two zones of actin filaments. Myo1p concentrates at the site of endocytosis and initiates a zone of actin filaments assembled by Arp2/3 complex. Wsp1p appears simultaneously at this site but subsequently moves away from the cell surface as it stimulates Arp2/3 complex to assemble a second zone of actin filaments. Cells lacking either nucleation-promoting factor assemble only one, stationary, zone of actin filaments. These observations support our two-zone hypothesis to explain endocytic tubule elongation and vesicle scission in fission yeast.**

Monitoring Editor
David G. Drubin
University of California, Berkeley

Received: Jun 21, 2017
Revised: Nov 28, 2017
Accepted: Nov 28, 2017

INTRODUCTION

Clathrin-mediated endocytosis recycles membrane receptors and takes up nutrients. Studies of budding yeast, fission yeast, and animal cells identified many proteins that assemble and disassemble at endocytic sites. Recruitment of membrane proteins that recognize the endocytic cargo initiates the process at nascent endocytic sites. These sites mature with the assembly of a clathrin coat and recruitment of nucleation promoting factors and Arp2/3 complex that stimulate actin polymerization. Yeast cells use mechanical force provided by actin polymerization to overcome the internal turgor pressure and deform the membrane (Aghamohammadzadeh and Ayscough, 2009; Minc *et al.*, 2009; Schaber *et al.*, 2010; Basu *et al.*, 2014).

However, it is still unclear how actin polymerization generates force to reshape the membrane, because conventional fluorescence microscopy has not resolved the organization of actin filaments or established the sites of actin polymerization. One model based on the localization of the nucleation promoting factors, myosin-I and WASp (Las17) in budding yeast, proposes that the actin filaments polymerize against the plasma membrane at the neck of endocytic invaginations. Consequently, the barbed ends of the elongating actin filaments are oriented toward the plasma membrane at the base of the membrane invagination with their pointed ends anchored to the clathrin coat via the adapter proteins at the invagination tip (Kaksonen *et al.*, 2005; Skruzny *et al.*, 2012; Picco *et al.*, 2015). Actin polymerization primarily at the plasma membrane together with some myosin motor activity is proposed to generate force to elongate the membrane tubule.

On the basis of the localization of the nucleation promoting factors in fission yeast, we proposed another model to explain how actin polymerization drives endocytosis (Arasada and Pollard, 2011). In our model, actin polymerization occurs in two distinct zones: one

This article was published online ahead of print in MBoC in Press (http://www.molbiolcell.org/cgi/doi/10.1091/mbc.E17-06-0415) on December 6, 2017.

*Address correspondence to: Thomas D. Pollard (thomas.pollard@yale.edu).

Abbreviations used: ARPC5, Arp2/3 complex subunit 5; CHD, calponin homology domain; DIC, differential interference contrast; EMM5S, Edinburgh minimal medium 5 supplements; Fim, fimbrin; FPALM, fluorescence photoactivation localization microscopy; mEGFP, monomeric enhanced green fluorescent protein; Myo1p, myosin-I; PALM, photoactivated localization microscopy; sCMOS, scientific complementary metal-oxide-semiconductor; STORM, stochastic optical reconstruction microscopy; Wsp1p, Wiskott-Aldrich syndrome protein.

at the base of the membrane invagination and the other traveling with the tip of the invagination. This model postulates that the expanding actin networks in the two zones repel each other as they grow, driving invagination of the plasma membrane tubule.

This two-zone model is based on quantitative measurements by confocal fluorescence microscopy of fission yeast actin patch proteins fused to mEGFP or mYFP (Sirotkin *et al.*, 2010; Arasada and Pollard, 2011). Two activators of Arp2/3 complex, type-I myosin Myo1p and WASp homologue Wsp1p, localize and initiate actin polymerization together but then separate with Myo1p at the base of plasma membrane invagination and Wsp1p at the tip of the invagination (Figure 1A). These nucleation promoting factors recruit very high densities (~20,000 molecules per μm^2) of two F-BAR (Fes/CIP4 homology Bin-Amphiphysin-Rvs) proteins, Cdc15p and Bzz1p, onto the invaginating membrane tubule. Cdc15p interacts with Myo1p at the base of the membrane tubule and Bzz1p interacts with Wsp1p at the invagination tip. The F-BAR proteins interact with the nucleation promoting factors to stimulate Arp2/3 complex in two zones along the invaginating tubule. However, in yeast cells expressing GFP-actin or GFP-tagged proteins that bind actin filaments, the dense network of ~5000 polymerized actin molecules appears as a single mass of homogeneous fluorescence ~500 nm in diameter at sites of endocytosis rather than as two distinct polymerization zones (Arasada and Pollard, 2011). Better spatial resolution was required to determine whether actin polymerizes in two zones.

Since the two yeast cells diverged from a common ancestor ~400 million years ago and have adapted differently during their subsequent evolution, they may control actin assembly during endocytosis in different ways. On the other hand, it is worth considering whether endocytosis in the two yeasts has more in common than suggested by these two models.

We used high-speed fluorescence photoactivation localization microscopy (FPALM) of live *Schizosaccharomyces pombe* cells expressing photoconvertible fluorescent proteins (Huang *et al.*, 2013; Laplante *et al.*, 2016a,b) to study the organization of proteins in actin patches. We obtained 1-s temporal resolution and ~35-nm spatial resolution and observed that actin filaments assemble in two zones: one at the base of the membrane invagination and the other at the tip of the invagination. Polymerization of actin in both zones depends on Arp2/3 complex, which is activated by type-I myosin Myo1p at the base of the invagination and WASp homologue Wsp1p along the path of the invagination from the cell surface to the tip of the membrane tubule. These observations support the two-zone hypothesis for the assembly of actin in association with endocytosis in fission yeast.

RESULTS

Observations of protein turnover in actin patches of live fission yeast cells by FPALM

We examined actin filaments and four components of the actin assembly machinery in live fission yeast using a single-molecule, superresolution method, FPALM (also called STORM or PALM) (Huang *et al.*, 2013; Laplante *et al.*, 2016a). We tagged proteins with the photoconvertible fluorescent proteins mMaple3 or mEOS3.2 at their gene loci unless indicated otherwise. The cell in Figure 1, B and C expressed the actin patch component capping protein Acp2p tagged with mEOS3.2. We used epifluorescence illumination to expose live *S. pombe* cells expressing photoconvertible fluorescent proteins continuously with both a near UV laser (405 nm) to photoconvert the fluorescent proteins randomly to the state that emits red light and a yellow laser (564 nm) to image the red light emitted by individual, spatially separated, photoconverted fluorescent proteins.

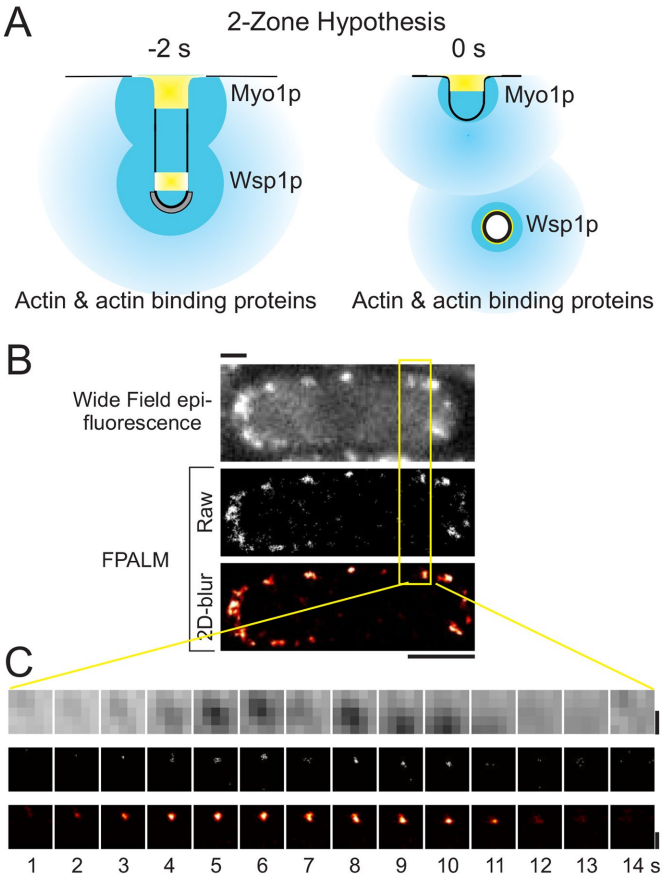

FIGURE 1: FPALM improves the spatial resolution of actin patches over conventional fluorescence microscope. (A) Two-zone model based on quantitative confocal fluorescence microscopy. The cartoon represents an actin patch at –2 s when the membrane tubule elongates and at 0 s when the vesicle pinches away from the plasma membrane. The plasma membrane is a black line, the clathrin coat is gray, nucleation-promoting factors Wsp1p and Myo1p are yellow, and zones with actin filaments are blue. Growth of the branched filaments from two distinct zones of NPFs is postulated to push the tip of the invaginating tubule away from the cell surface contributing to the elongation of the tubule and scission of the coated vesicle. (B, C) Fluorescence micrographs of an *S. pombe* cell expressing capping protein Acp2p-mEOS3.2 with focusing in the middle plane of the cell. We used continuous epifluorescence illumination to photoconvert mEOS3.2 with 405- and 564-nm lasers to excite the photoconverted mEOS3.2 through the entire cell. Top panels, wide-field epifluorescence images reconstructed from the total fluorescence emission. Middle panels, raw FPALM images constructed from the localizations of single molecules. Bottom panels, each localized emitter in the raw data set was convolved with a Gaussian kernel (σ = 1.5 pixel) and color coded for density in a heat map. (B) Whole cell during a 1-s interval. Scale bar is 1 μm. (C) Time series of images of one actin patch at 1-s intervals each reconstructed from 200 sequential frames. Top panel, inverted contrast wide-field epifluorescence images. Scale bar is 250 nm.

Over time, all of the fluorescent proteins within the ~400-nm-thick imaging plane were localized with an average radial precision of 21 ± 4 nm, and the centroids of each molecule were plotted as two-dimensional histograms (Figure 1B, middle panel). Software rejected molecules outside the imaging plane during image processing. To aid visualization the two-dimensional histograms of centroids of

localized molecules were convolved with a two-dimensional Gaussian kernel (σ = 7.5 nm) and color coded for localization density (Figure 1B, bottom panel).

It is important to note that photoactivation localization microscopy depends on irreversibly photobleaching each fluorescent protein after it is imaged and localized, so a time series of FPALM images reveals the position of each molecule when it is photoconverted. Photobleaching occurs in less than 2 s under our conditions (Laplante *et al.*, 2016b). However, the method does not reveal the subsequent history of the photobleached protein, such as its persistence at the site of localization or any motion.

Actin patches concentrate at the poles of the cells but are spread around the surface, so they are viewed from many different angles. Therefore, we used differential interference contrast (DIC) microscopy to identify the midplane of the cells, where actin patches moving in the *XY*-plane of the microscope were contained in the optical section throughout their lifetimes. To obtain enough single-molecule localizations to form an image, we combined groups of 200 sequential 5-ms frames. These 1-s composite images were linked into movies or montages to show actin patch dynamics. These FPALM images highlight structural details of actin patches that appear as blurred, pixelated spots of fluorescence by wide-field fluorescence microscopy (Figure 1C, top panel).

Localization of Arp2/3 complex activators and Arp2/3 complex

We tagged three proteins that control the assembly of actin filaments at sites of endocytosis and established their distributions over time in actin patches. We inserted the open reading frame for mMaple3 (Wang *et al.*, 2014) into the genome so the fluorescent protein was fused to the N-termini of Arp2/3 complex activators myosin-I (Myo1p) and Wiskott-Aldrich syndrome protein (Wsp1p) and on the C-terminus of the Arc5p (ARPC5) subunit of Arp2/3 complex, so all of the tagged proteins were expressed from their endogenous promoters. *Schizosaccharomyces pombe* cells expressing these fusion proteins were viable and had wild-type morphologies at 25° and 36°C.

In wild-type cells, localizations of mMaple3-Myo1p appeared in a small, stationary region 65 ±18 nm (mean ± SD) wide and extending 85 ±18 nm from the plasma membrane (Figure 2, A, C, and D, left graphs) as actin patches assembled and disassembled over time (Figure 2A, top panel). A composite image with temporal color coding according to the time of localization shows the time course of the whole process (Figure 2B, left micrograph). Counts of mMaple3-Myo1p localizations in actin patches over time established that 82% of Myo1p localizations appeared and disappeared within membrane proximal zone (defined as box ~250 nm wide, extending 200 nm into the cytoplasm from the cell edge) (left panels in Figure 2B and and Supplemental Figure S1A). These observations confirmed at much higher resolution the lack of mobility of Myo1p tagged with mEGFP (monomeric enhanced green fluorescent protein) and imaged by confocal microscopy (Sirotkin *et al.*, 2005, 2010).

Over ~15 s, mMaple3-Wsp1p appeared at the plasma membrane and subsequently was localized along a trajectory normal to the membrane (middle column of Figure 2, B–E), similarly to lower-resolution confocal micrographs of cells expressing mEGFP-Wsp1p (Sirotkin *et al.*, 2010). Reconstructions of time series with temporal color-coding illustrate that mMaple3-Wsp1p molecules were localized up to 300 nm from the plasma membrane at late time points (Figure 2B, center micrograph). The clusters of mMaple3-Wsp1p maintained a constant size with a width of 100 ± 38 nm and length of 200 nm (Figure 2, C and D, center graphs) as they moved from the membrane proximal zone to the membrane distal zone (a box ~250 nm wide located in the cytoplasm between 200 and 550 nm from the cell edge) (Figure 2E, middle panel, and Supplemental Figure S1B). mMaple3-Wsp1p appeared in the membrane proximal zone and peaked there at ~50 localizations per second. The peak of ~50 mMaple3-Wsp1p localizations per second in the membrane distal zone was ~6 s later.

The localizations of Arc5p-mMaple3 (the marker for Arp2/3 complex) appeared first at the plasma membrane and then deeper in the cytoplasm at later times (Figure 2A, bottom panel), as illustrated by composite images with temporal color coding (Figure 2B, right micrograph). Throughout this shift in the localizations over time, clusters of Arc5p-mMaple3 were 122 ± 62 nm wide and 300 nm long (Figure 2, C and D, right panels). Like mMaple3-Wsp1p, the localizations of Arc5p-mMaple3 molecules first peaked at ~150 per second in the membrane proximal zone followed ~5 s later by a peak in membrane distal zone (Figure 2E, right panel, and Supplemental Figure S1C).

Actin assembles in two distinct zones in an actin patch

We localized actin filaments indirectly with two different probes: 1) an actin filament binding protein fimbrin (Fim1p) tagged to mEOS3.2 at its C-terminus and expressed from the endogenous locus; and 2) calponin homology domain (CHD) from the *S. pombe* IQGAP protein Rng2p fused to mEOS3.2 at its N terminus and expressed ectopically from a repressible promoter at the *leu1*$^+$ locus (Figure 3). Fim1p-mEOS3.2 expressed from the native promoter has minimal impact on the organization of actin filaments at endocytic sites (Berro and Pollard, 2014b,a). CHD tagged with a fluorescent protein binds actin filaments, but it also appears to bundle actin filaments and may influence cell morphology when overexpressed. The time course of the appearance and disappearance of Fim1p-mEOS3.2 in patches (Figure 3H) was similar to a trace of Fim1p-mGFP or Fim1p-mCherry observed by confocal microscopy (Sirotkin *et al.*, 2010; Berro and Pollard, 2014a).

Both actin filament probes appeared in two distinct zones at sites of endocytosis (Figure 3, A and B), first close to the plasma membrane and then in a second zone further from the plasma membrane. Throughout their existence, the clusters of single molecule localizations of mEOS3.2-CHD in patches were 110 ± 55 nm wide (along the cell long axis) and 350 nm long, while those of Fim1p-mEOS3.2 were 101 ± 36 nm wide and 300 nm long, both with two distinct peaks (Figure 3, C– F). Reconstructions of series of images (Figure 3A) with temporal color-coding emphasize that actin assembly begins at the plasma membrane and shifts to a site deeper in the cytoplasm over time (Figure 3, G and H). Like Arp2/3 complex, the mEOS3.2-CHD and Fim1p-mEOS3.2 first peaked at ~150 localizations per second in the membrane proximal zone followed ~4 s later by a peak in the membrane distal zone (Figure 3, I and J, and Supplemental Figure S1, D and E).

Starting at time 0 s, the localizations of each actin patch protein declined and appeared further from the plasma membrane. At the onset of patch assembly and up to time zero, the localizations of the patch proteins were tightly packed in a column normal to the plasma membrane. After time zero, the positions of these localizations became more variable and more spread out. The localizations colored in red at the end of the disassembly phase were more spread out and noisy due to fewer localizations.

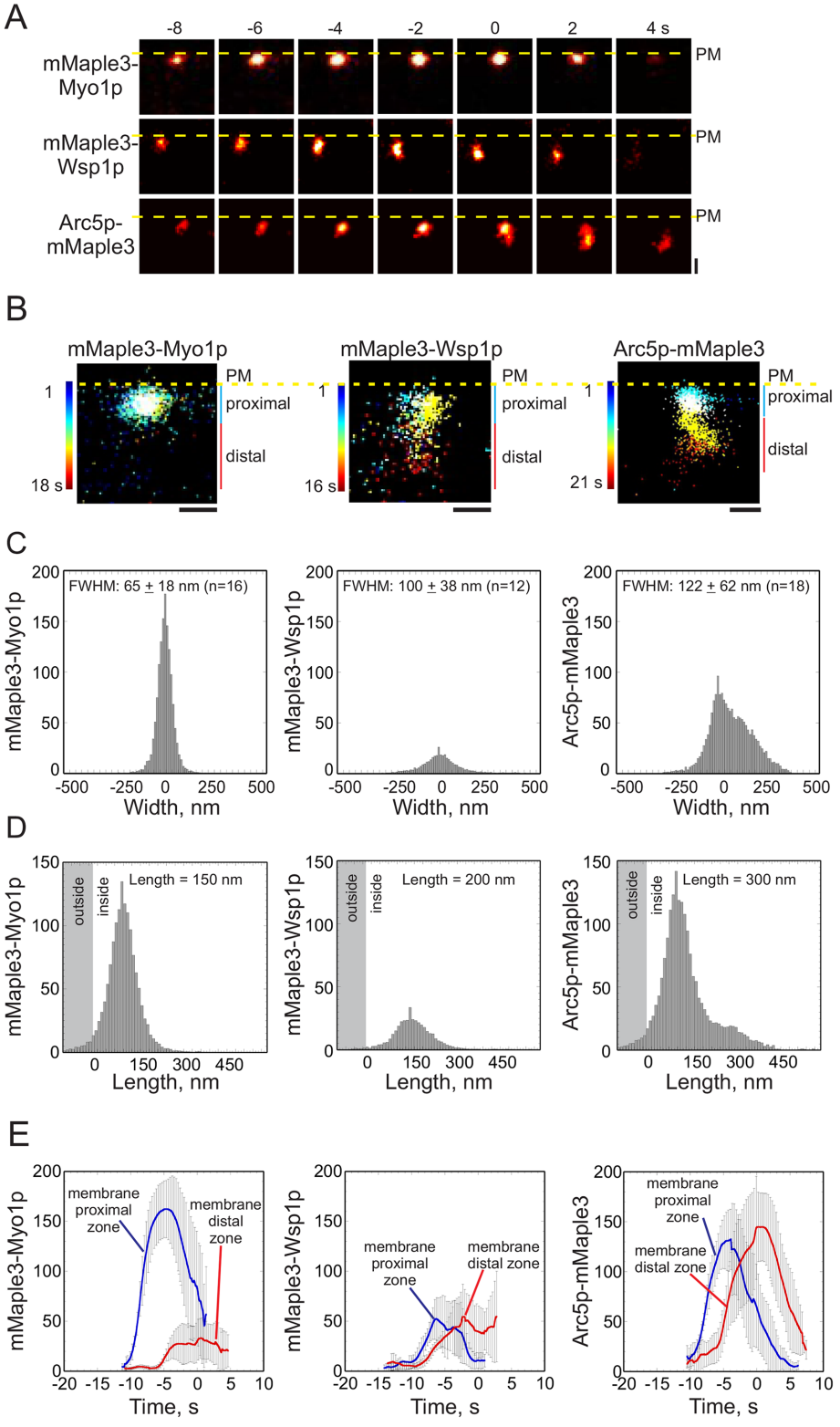

FIGURE 2: Localization of nucleation promoting factors and Arp2/3 complex in actin patches by FPALM in wild-type cells. (A) Time series of FPALM images color coded for the density of localizations: top, mMaple3-Myo1p; middle, mMaple3-Wsp1p; and bottom, Arc5p-mMaple3 a subunit of Arp2/3 complex. The micrographs were aligned to time 0 s when the vesicle pinches away from the plasma membrane. For mMaple3-Myo1p the peak localizations were aligned to the peak localizations of mMaple3-Wsp1p. Yellow dashed lines show the position of the plasma membrane. Scale bar is 100 nm. (B) Composite images with temporal color coding of single molecule localizations over the lifetimes of single actin patches: left, 18 s from a cell expressing mMaple3-Myo1p; center, 16 s from a cell expressing mMaple3-Wsp1p; and right, 21 s from a cell expressing Arc5p-mMaple3 a subunit of Arp2/3 complex. The blue and red lines indicate the membrane-proximal and membrane-distal regions. Scale bar is 200 nm. (C, D) Spatial distributions of single molecule localizations in FPALM images of actin patches. FWHM is full-width of the distributions at half-maximums. (C) Width distributions and (D) length distributions of localizations of left, mMaple3-Myo1p in 20 actin patches; center, mMaple3-Wsp1p in 12 actin patches; and right, Arc5p-mMaple3 in 18 actin patches. The data from separate patches were aligned to their peaks and averaged. Full-widths at half-maximum were calculated from the distributions of the localizations along the *x*-axis. The lengths of the patches are given as the distances that include 90% of the localizations from the cell edge. The gray area in the graphs represents the localizations detected outside the cell. (E) Time courses of the average number of localizations detected in (blue line) the membrane proximal zone (200 × 250-nm region next to the cell edge) and (red line) the membrane distal zone (350 × 250-nm region 200 nm away from the cell edge): left, mMaple3-Myo1p; middle, mMaple3-Wsp1p; and right, Arc5p-mMaple3. Raw time courses of the number of emitters localized in 15 actin patches were aligned to a reference patch and averaged to produce time courses for the average number of localizations. Mean total localizations were used to align the localizations in the membrane proximal and distal zone on the same time scale as the numbers of GFP molecules assembled in actin patches. Time 0 s indicates vesicle scission. Error bars are SDs. Every third error bar is shown.

Assembly of two zones of actin is required for endocytic tubule elongation and vesicle scission from the plasma membrane

Both Myo1p and Wsp1p contribute to activating Arp2/3 complex and the assembly actin filaments at sites of endocytosis in fission yeast. Both Δ*wsp1* and Δ*myo1* mutant cells are viable with defects in endocytosis, but double mutant Δ*wsp1*Δ*myo1* cells are not viable (Lee *et al.*, 2000; Sirotkin *et al.*, 2005). We investigated the relationships among Myo1p, Wsp1p, Arp2/3 complex, and actin filaments by analyzing Δ*wsp1* yeast cells lacking Wsp1p or Δ*myo1* cells lacking Myo1p (Figure 4). We compared the distribution of Arc5p-mMaple3 and mEOS3.2-CHD in the mutant strains with wild-type cells.

Both single deletion strains differed from wild-type cells in two regards: 1) they accumulated far less Arc5p-mMaple3 than

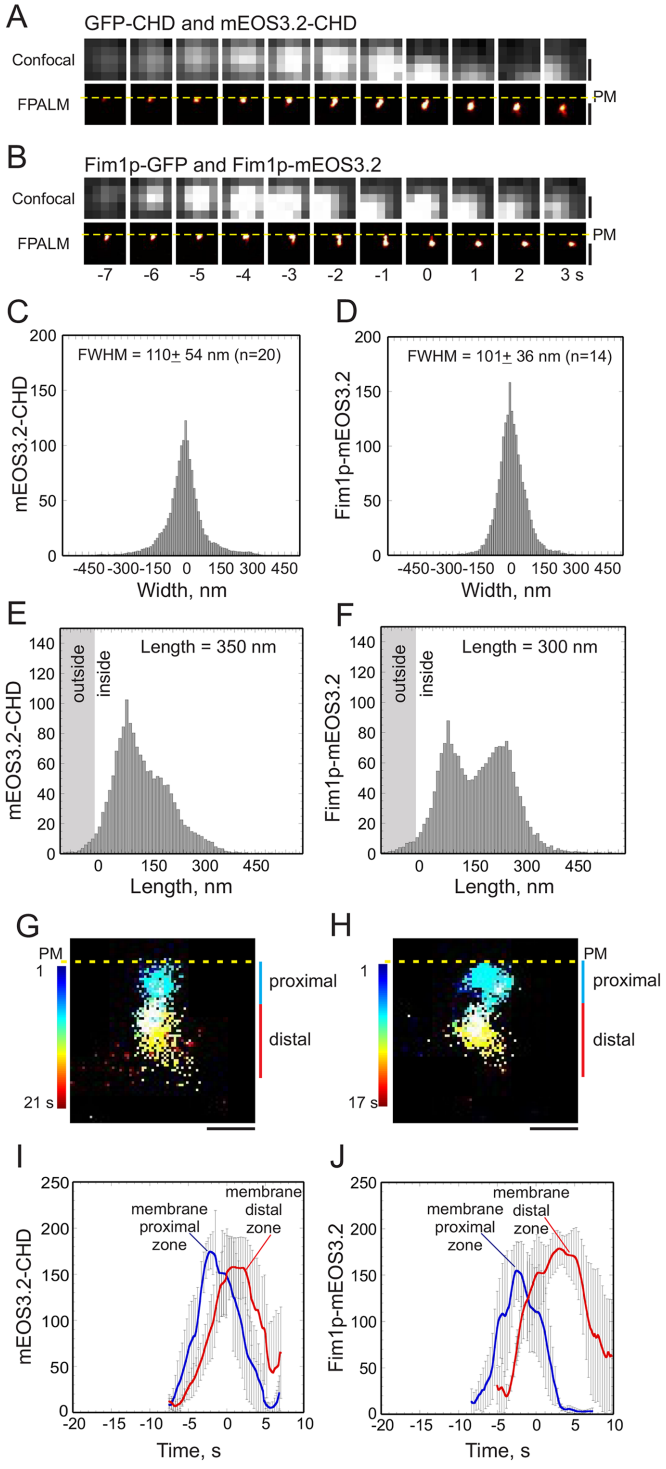

FIGURE 3: Localization of actin filaments in two zones in endocytic actin patches in wild-type *S. pombe* cells. (A, B) Time series of fluorescence micrographs at 1-s intervals of representative actin patches in cells expressing proteins that bind actin filaments. The images are regions of interest of ~500 × 500 nm around one actin patch for each protein. Scale bars are 250 nm. (A) GFP-CHD and mEOS3.2-CHD and (B) Fim1p-GFP and Fim1p-mEOS3.2. Top panels, maximum intensity projections of five confocal *z*-slices in the *XY*-plane of individual actin patches from cells expressing GFP-CHD or Fim1p-GFP. Bottom panels, FPLAM images of cells expressing mEOS3.2-CHD or Fim1p-mEOS3.2. Each localized emitter was convolved with a Gaussian kernel ($\sigma = 1.5$ pixel) and color coded for density in a heat map. Yellow dashed lines show the location of the plasma membrane (PM). (C–F) Spatial distributions of single molecule localizations of mEOS3.2-CHD and Fim1p-mEOS3.2 in FPALM images of actin patches. FWHM is full-width of the distributions at half-maximums. (C) Width distribution and (E) length distribution of mEOS3.2-CHD in 20 actin patches. (D) Width distribution and (F) length distribution of Fim1p-mEOS3.2 in 14 actin patches prepared as in Figure 2. (G, H) Composite images with temporal color coding of single molecule localizations over the lifetimes of single actin patches. The micrographs are aligned to time 0 s when the vesicle pinches off from the plasma membrane. Scale bars are 200 nm. The blue and red lines indicate the membrane-proximal and membrane-distal regions. (G) Twenty-one seconds from a cell expressing mEos3.2-CHD. (H) Seventeen seconds from a cell expressing Fim1p-mEos3.2. (I, J) Time courses of the average number of localizations of (I) CHD-mEOS3.2 and (J) Fim1p-mEOS.2 detected in (blue line) the membrane proximal zone (200 × 250-nm region next to the cell edge) and (red line) the membrane distal zone (350 × 250-nm region 200 nm away from the cell edge). Raw time courses of the number of emitters localized in 15 actin patches were aligned to a reference patch and averaged to produce time courses for the average number of localizations. Time zero seconds indicates vesicle scission. Mean total localizations were used to align the localizations in the membrane proximal and distal zone on the same time scale as the numbers of GFP molecules assembled in actin patches. Error bars are SDs. Every third error bar is shown.

wild-type cells (Figure 4A); and 2) the localizations of Arc5p-mMaple3 appeared and remained next to the plasma membrane (Figure 4, A and B) as actin patches assembled and disassembled over time. Thus, few Arc5p-mMaple3 molecules were localized in the membrane distal zone at any time (Figure 4E and Supplemental Figure S2A).

In cells lacking either Myo1p or Wsp1p, the actin filament marker mEOS3.2-CHD remained close to the plasma membrane and persisted there longer than in wild-type cells (Figure 4F and Supplemental Figure S2B). The peak numbers of mEOS3.2-CHD localizations in membrane proximal zones of actin patches were similar in wild-type cells and cells without Myo1p or Wsp1p, but few of the localizations appeared in the membrane distal zone.

DISCUSSION

High-speed FPALM increases the spatial resolution nearly 10-fold compared with confocal microscopy and is fast enough to follow the assembly and disassembly of actin patches. We used the established timing of GFP-tagged proteins (Sirotkin *et al.*, 2010; Arasada and Pollard, 2011) to align the timing of the superresolution microscopy data, with 0 s as the time when some of the patch components start to move away from the cell surface after vesicle scission (Figure 5). High-resolution images aligned in this way at 1-s intervals helped us distinguish elongation of the membrane tubule from vesicle scission and support the two-zone hypothesis.

Note that after random photoconversion FPALM irreversibly bleaches each fluorescent protein in the imaging beam in ~2 s (Laplante *et al.*, 2016b), so the method does not reveal how long each molecule persists at its detected location. Thus, the absence of localizations does not necessarily mean that the tagged protein has turned over. For example, actin may persist longer in the membrane proximal zone than the detection of newly localized proteins.

Status of the two-zone hypothesis

The key feature of the two-zone hypothesis is that the two major nucleation promoting factors, Myo1p and Wsp1p, are distributed differently on the membrane tubules, so they can drive the reactions

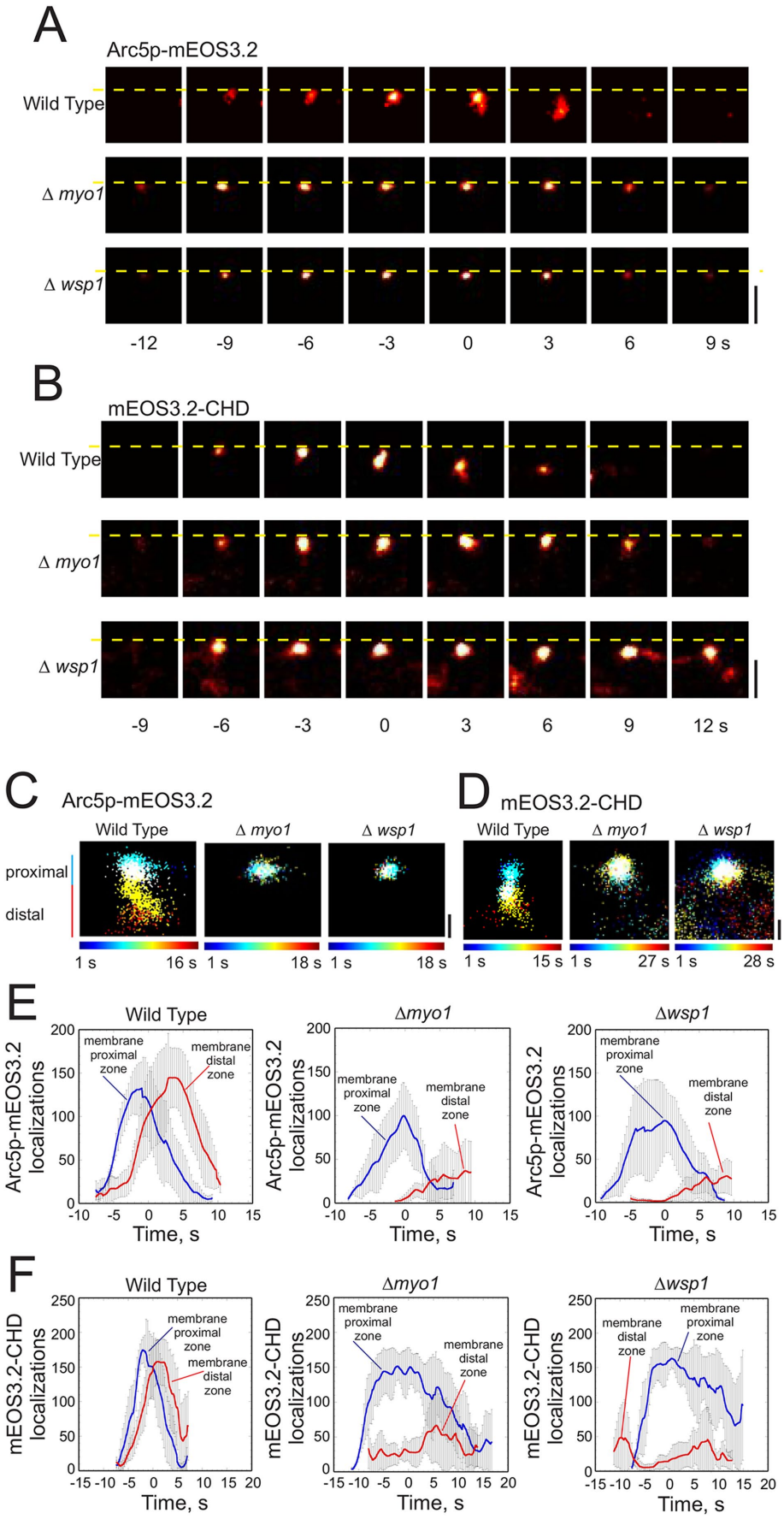

that produce two zones of actin polymerization. Confocal microscopy showed that Myo1p and Wsp1p have lifetimes of ~15 s in actin patches. They appear at the same time, peak together at time –3 s with ~165 molecules of Myo1p and ~140 molecules of Wsp1p, and disappear together around time +6 s (Sirotkin *et al.*, 2010; Arasada and Pollard, 2011). Superresolution images show that Myo1p is stationary at the base of the membrane invagination, while Wsp1p first appears at the same place as Myo1p followed by new localizations further from the plasma membrane. This relocation of

FIGURE 4: Actin patch assembly in cells lacking nucleation promoting factors Myo1p or Wsp1p. (A, B) Time series of FPALM images color coded for localization density showing the (A) Arc5p-mMaple3 a subunit of Arp2/3 complex or (B) mEOS3.2-CHD to visualize actin filaments. Top panels, wild-type cells; middle panels, Δ*myo1* cells; and bottom panels, Δ*wsp1* cells. Yellow dotted lines indicate the cell membrane. The micrographs are aligned to time 0 s when the vesicle pinches off from the plasma membrane. Scale bars are 250 nm. (C, D) Composite images with temporal color coding of single molecule localizations over the lifetimes of single actin patches. The blue and red lines indicate the membrane-proximal and membrane distal regions. (C) Cells expressing Arc5p-mMaple3: left, 16 s of an actin patch in a wild-type cell; center, 18 s of an actin patch in a Δ*myo1* cell; and right, 18 s of an actin patch in a Δ*wsp1* cell. (D) Cells expressing mEOS3.2-CHD: left, 15 s of an actin patch in a wild-type cell; center, 27 s of an actin patch in a Δ*myo1* cell; and right, 28 s of an actin patch in a Δ*wsp1* cells. (E, F) Time courses of the average number of localizations of (E) Arc5p-mMaple3 and (F) mEOS.2-CHD detected in actin patches in (blue line) the membrane proximal zone (200 × 250-nm region next to the cell edge) and (red line) the membrane distal zone (350 × 250-nm region 200 nm away from the cell edge): left, wild-type cells; middle, Δ*myo1* cells; and right, Δ*wsp1* cells. Raw time courses of the number of emitters localized in 15 actin patches were aligned to a reference patch and averaged to produce time courses for the average number of localizations. Mean total localizations were used to align the localizations in the membrane proximal and distal zone on the same time scale as the numbers of GFP molecules assembled in actin patches. Time 0 s indicates the vesicle scission. Error bars are SDs. Every third error bar is shown.

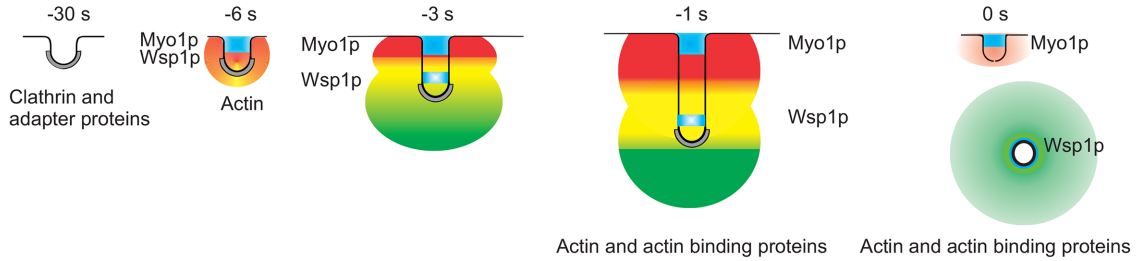

FIGURE 5: Hypothesis for the contributions of the nucleation promoting factors Myo1p and Wsp1p to endocytosis. Different stages of endocytosis with time zero defined as vesicle scission from the plasma membrane. The plasma membrane is a black line, clathrin is gray, nucleation promoting factors Wsp1p and Myo1p are blue, and actin filaments are red, green, and yellow. Clathrin is recruited 2 min prior to invagination. Nucleation promoting factors are recruited beginning at –6 s and peak prior to patch movement at –3 s. Myo1p and Wsp1p both stimulate actin polymerization at the base of the invagination near the cell surface. As the actin zones around Myo1p and Wsp1p grow, they repel each other, driving membrane invagination and redistribution of Wsp1p away from the base along the membrane invagination creating new sites of actin polymerization at the invagination tip. Myo1p remains associated with the plasma membrane at the base of the invagination. The expansion of the two zones triggers vesicle scission between the two zones of actin at time 0 s.

Wsp1p begins at time –3 s coincident with the peak of Wsp1p localizations and the accumulation of localizations in the membrane distal zone of Arp2/3 complex (Arc5p) and actin filaments (CHD and Fim1p). Localizations of both Arp2/3 complex and actin filaments peak at time 0 s. Both Arp2/3 complex (Figure 3B) and actin (Figure 2, H and I) form two spatially and temporally separated networks of about the same size.

Judging from their sudden increase in mobility, patches pinch off from the membrane with most of the actin network at time 0 s (Berro and Pollard, 2014b,a). After time 0, patches diffuse in the cytoplasm at increasing rates as they disassemble their actin filament coat over 6 s (Berro and Pollard, 2014b,a). Localizations of Arc5p, CHD, and Fim1p decline more rapidly in the membrane proximal zone than the membrane distal region. These proteins may dissociate from the patch or persist after they are localized. The sudden collapse of the membrane tubule after vesicle scission might be a factor in dispersing the actin.

How much does endocytosis in fission and budding yeast have in common?

In spite of differences in a few observations, most evidence supports the conclusion that the mechanisms of endocytosis in budding yeast and fission yeast are fundamentally the same. The two yeasts have a common ancestor and use most of the same proteins to form a membrane invagination ~150 nm long surrounded by actin filaments (Kaksonen *et al.*, 2005; Sirotkin *et al.*, 2010; Arasada and Pollard, 2011; Goode *et al.*, 2015; Lu *et al.*, 2016). Actin polymerization in both yeasts depends on Arp2/3 complex and two types of nucleation promoting factors, myosin-I (MYO3 and MYO5 in budding yeast and Myo1p in fission yeast) and WASp homologues (LAS17 in budding yeast and Wsp1p in fission yeast).

In both the yeasts, myosin-I appears near the plasma membrane at the base of the tubular invagination (Kaksonen *et al.*, 2005; Sun *et al.*, 2006; Galletta *et al.*, 2008; Idrissi *et al.*, 2008; Sirotkin *et al.*, 2010) and recruits Arp2/3 complex to nucleate branched actin filaments that give rise to the membrane-proximal network of filaments. In both yeasts, interactions of myosin-Is with adapter and coat proteins (Sun *et al.*, 2006; Barker *et al.*, 2007; Arasada and Pollard, 2011) are important for efficient endocytosis. For example, recruitment of F-BAR protein Cdc15p to the endocytic site enhances the ability of Myo1p to stimulate actin polymerization by Arp2/3 complex in fission yeast (Arasada and Pollard, 2011) and phosphorylation of the Myo1p TEDS site (Serine 361) by Pak1p appears to be the upstream signal that localizes Myo1p at clathrin-coated pits (Attanapola *et al.*, 2009). In both yeasts, WASp initially concentrates near the plasma membrane and recruits the F-BAR protein Bzz1p, which increases the ability of Wsp1p to activate Arp2/3 complex to assemble actin filaments (Padrick *et al.*, 2008; Arasada and Pollard, 2011).

The main difference is the subsequent behavior of WASp. The current work confirms that fission yeast Wsp1p moves away from the cell surface along with Arp2/3 complex and actin filaments (Arasada and Pollard, 2011), while multiple papers (Kaksonen *et al.*, 2005; Sun *et al.*, 2006, 2017; Rajmohan *et al.*, 2009; Picco *et al.*, 2015) show that budding yeast Las17-GFP remains close to the cell surface during endocytosis. Consistent with a single zone of nucleation promoting factors in budding yeast, elegant photobleaching experiments showed that actin filaments appear at the base of the membrane invagination (Picco *et al.*, 2015).

The accumulated work suggests that the behavior of WASp differs in the two yeasts, supporting a single zone of actin assembly in budding yeast and two zones in fission yeast. Exploring this difference is worthwhile for two reasons. First, tagging Las17 or Wsp1p can influence their behavior. Growth and the time course of patch assembly are normal in fission yeast cells dependent on mGFP-Wsp1p (Sirotkin *et al.*, 2005), rather than growing slowly like misshapen, temperature-sensitive Δ*wsp1* cells. However, the GFP-Wsp1p strain has defects in mating and sporulation, as observed in Δ*wsp1* cells. Tagging either end of Las17 with GFP may compromise patch mobility (Galletta *et al.*, 2008). Second, electron microscopy of sections of chemically fixed budding yeast cells treated with gold-labeled antibodies showed that Las17 with a small C-terminal HA peptide tag distributed significantly further than myosin-I along endocytic membrane invaginations as they elongated ($p < 0.001$). However, chemical fixation may have compromised the preservation. High-pressure freezing followed by freeze substitution improves the preservation and is compatible with antibody staining for electron microscopy (Buser and Drubin, 2013) or correlative fluorescence and electron tomography (Kukulski *et al.*, 2012), but neither Las17 nor myosin-I have been localized by these methods.

Models of actin assembly

Understanding the forces produced by actin assembly during endocytosis depends on knowing the sites of assembly and the orientations of the filaments. Electron microscopy of chemically fixed and freeze-substituted yeast cells (Idrissi *et al.*, 2008), platinum replicas of fixed and extracted animal cells (Collins *et al.*, 2011), and quantitative fluorescence microscopy of live cells (Kaksonen *et al.*, 2005; Sirotkin *et al.*, 2005, 2010; Berro *et al.*, 2010; Berro and Pollard, 2014b,a; Arasada and Pollard, 2011; Picco *et al.*, 2015) have suggested three possible orientations of filaments in actin patches as follows: 1) actin filaments are assembled from the plasma membrane with barbed ends oriented toward the plasma membrane (Kaksonen *et al.*, 2005; Picco *et al.*, 2015); 2) actin filaments are oriented with the barbed ends pointed toward the tip of the membrane invagination (Collins *et al.*, 2011); and 3) very short actin filaments (Young *et al.*, 2004; Kaksonen *et al.*, 2005; Sirotkin *et al.*, 2005, 2010; Berro *et al.*, 2010; Berro and Pollard, 2014b,a; Arasada and Pollard, 2011; Picco *et al.*, 2015) are oriented randomly in one zone (Young *et al.*, 2004; Kaksonen *et al.*, 2005; Sirotkin *et al.*, 2005, 2010; Berro *et al.*, 2010; Berro and Pollard, 2014b,a; Arasada and Pollard, 2011; Picco *et al.*, 2015) or two zones (Arasada and Pollard, 2011). Model 3 with two zones is simpler and more appealing to us, because it does not require mechanisms to orient the filaments. Distinguishing these hypotheses definitively will require methods to document the arrangement of individual filaments.

MATERIALS AND METHODS

Strain construction, growth conditions, and yeast methods

Supplemental Table S1 lists the *S. pombe* strains used in this study. Fluorescent protein (FP) tag sequences were integrated into the genome by PCR-based gene tagging (Bahler *et al.*, 1998). All genomic integrations were confirmed by PCR and fluorescence microscopy. We used plasmid pFA6a-mEos3.2-kanMX6 to tag proteins with mEOS3.2 at their endogenous genomic loci (Laplante *et al.*, 2016b). We constructed plasmid pFA6a-mMaple3-KanMX6 to tag proteins at their endogenous loci with mMaple3. mMaple3 cDNA was PCR amplified and replaced mEOS3.2 in pFA6a-mEos2-kanMX6. We constructed pFA6a-kanMX6-Pmyo1-mMaple3 and pFA6a-kanMX6-Pwsp1-mMaple3 plasmids for N-terminal tagging of Myo1p and Wsp1p. We PCR amplified the coding sequence of mMaple3 (Wang *et al.*, 2014) and replaced the mEGFP coding sequence of pFA6a-kanMX6-Pmyo1-mEGFP and pFA6a-kanMX6-Pmyo1-mEGFP using the restriction sites *Pac*I and *Asc*I (Sirotkin *et al.*, 2005). Actin filaments were visualized indirectly with either with Fim1p-mEOS3.2 or with Rng2p CHD. To express mEOS3.2-CHD or GFP-CHD, cells expressing mEOS3.2-CHD or GFP-CHD under the control of a 41x*nmt1* promoter were grown in Edinburgh minimal media (EMM5S) for 18 h before imaging.

Preparation of cells for imaging

All *S. pombe* cells expressing a fluorescently tagged protein were grown in YE5S at 25°C to OD_{595} 0.2–0.5, washed in EMM5S filtered through a 0.45-μm filter, and mounted on 25% gelatin pads in filtered EMM5S. DIC images were collected prior to superresolution imaging.

Superresolution data acquisition, data analysis, and display

Superresolution imaging was performed with a custom-built two-dimensional FPALM system (Huang *et al.*, 2013; Laplante *et al.*, 2016a,b) equipped with a scientific complementary metal-oxide-semiconductor (sCMOS) camera (ORCA-Flash4.0; Hamamatsu). Wide-field epifluorescence optics were used to illuminate cells simultaneously with a near-UV laser (405 nm) to photoconvert small numbers of random fluorescent proteins and 564-nm laser to excite the fluorophores through the entire cell. The average intensity of the 564-nm laser used to excite photoconverted mEOS3.2 and mMaple3 for imaging was ~1.2 kW/cm^2. To maintain an optimal density of photoconverted mEOS3.2 or mMaple3 for single molecule localization, the power of the 405-nm photoconversion laser was increased every 5 s during data acquisition with a computer-controlled ramp to compensate for irreversible photobleaching of molecules that were photoconverted and imaged. Single-molecule images were acquired at a frame rate of 200 frames/s for 40–60 s from the medial focal plane of a cell with an sCMOS camera (ORCA-Flash4.0; Hamamatsu) using HCimage software (Hamamatsu).

Acquired frames were analyzed using a custom sCMOS-specific localization algorithm based on a maximum likelihood estimator (Huang *et al.*, 2013; Laplante *et al.*, 2016a,b). Localizations were plotted to construct a two-dimensional histogram FPALM image. To aid visualization of the two-dimensional histogram images, the images were convolved with a two-dimensional Gaussian kernel (σ = 7.5 nm). Time-lapse images showing dynamics were built by combining sequential 200 frame reconstructions (1-s intervals) and color coded for localization density. To display temporal information in a single composite image, the localizations in each 1-s time point was assigned a Matlab Jet Color over the lifetime of the patch. We extracted from the Matlab images of individual patches the numbers of localized emitters detected each second overall and from two spatial zones. Dimensions of an immobile mMaple3-Myo1p patch that is confined the plasma membrane is used as a reference for the membrane proximal zone. Most of the mMaple3-Myo1p localizations are confined to a region 250 nm wide and 200 nm deep from the cell edge. Localizations that were detected within a 250-nm-wide and 200-nm-deep box from the cell edge were classified as membrane proximal zone, and any localizations detected outside the region are defined to be in the membrane distal region. The membrane distal region is limited to 250 nm wide and 350 nm deep starting 200 nm away from the cell edge. Images acquired in each data set (typically 38–40 s at 200 frames/s) were sum projected, and the boundary of the localizations was identified as the cell edge. The raw time courses were aligned to the time course of a reference patch using the temporal superresolution realignment method (Berro and Pollard, 2014a) and averaged to obtain the average time course of localized emitters in the membrane proximal and membrane distal regions. The time courses were aligned to the vesicle scission event at time 0 s. To align the data, we first obtained the time courses of the total number of localizations detected in the actin patch (sum localizations in the membrane proximal region and in the membrane distal regions). We then aligned the peak number of localizations detected to the peak number of GFP/YFP molecules assembled in an actin patch reported previously (Sirotkin *et al.*, 2010; Arasada and Pollard, 2011).

To measure the dimensions of the actin patch, a 100 × 100 pixel region with an actin patch was selected, and the coordinates of the localizations for the patch were calculated from the 100 × 100 two-dimensional matrix using Matlab. The patches in all of the figures were oriented with the cell surface at the top with the cell interior below. DIC images acquired prior to FPALM imaging were used to align patches in this coordinate system. To calculate the width of the patch, localization densities in each column of the two-dimensional matrix were summed and projected onto an *x*-axis. The width of the patch represents the width of the localization density distribution at half the maximum. To calculate the length of the patch, localization

densities in each row of the two-dimensional matrix were summed and projected onto a *y*-axis. The length of the patch is the distance that includes 90% of the localizations from the cell edge. To align data from multiple patches, we defined the cell edge as the position with 10% the peak number of localizations. The length distributions of the aligned patches were averaged.

ACKNOWLEDGMENTS

Research reported in this publication was supported by the National Institute of General Medical Sciences of the National Institutes of Health under award numbers R01GM026132 and R01GM026338 to T.D.P. and grant R01GM115636 to J.B. The content is solely the responsibility of the authors and does not necessarily represent the official views of the National Institutes of Health. We thank Steven Wang for providing a plasmid with mMaple3 and especially Jeorg Bewersdorf of Yale University for the use of his superresolution microscope.

REFERENCES

Aghamohammadzadeh S, Ayscough KR (2009). Differential requirements for actin during yeast and mammalian endocytosis. Nat Cell Biol 11, 1039–1042.

Arasada R, Pollard TD (2011). Distinct roles for F-BAR proteins Cdc15p and Bzz1p in actin polymerization at sites of endocytosis in fission yeast. Curr Biol 21, 1450–1459.

Attanapola SL, Alexander CJ, Mulvihill DP (2009). Ste20-kinase-dependent TEDS-site phosphorylation modulates the dynamic localisation and endocytic function of the fission yeast class I myosin, Myo1. J Cell Sci 122, 3856–3861.

Bahler J, Wu JQ, Longtine MS, Shah NG, McKenzie A 3rd, Steever AB, Wach A, Philippsen P, Pringle JR (1998). Heterologous modules for efficient and versatile PCR-based gene targeting in Schizosaccharomyces pombe. Yeast 14, 943–951.

Barker SL, Lee L, Pierce BD, Maldonado-Baez L, Drubin DG, Wendland B (2007). Interaction of the endocytic scaffold protein Pan1 with the type I myosins contributes to the late stages of endocytosis. Mol Biol Cell 18, 2893–2903.

Basu R, Munteanu EL, Chang F (2014). Role of turgor pressure in endocytosis in fission yeast. Mol Biol Cell 25, 679–687.

Berro J, Pollard TD (2014a). Local and global analysis of endocytic patch dynamics in fission yeast using a new "temporal superresolution" realignment method. Mol Biol Cell 25, 3501–3514.

Berro J, Pollard TD (2014b). Synergies between Aip1p and capping protein subunits (Acp1p and Acp2p) in clathrin-mediated endocytosis and cell polarization in fission yeast. Mol Biol Cell 25, 3515–3527.

Berro J, Sirotkin V, Pollard TD (2010). Mathematical modeling of endocytic actin patch kinetics in fission yeast: disassembly requires release of actin filament fragments. Mol Biol Cell 21, 2905–2915.

Buser C, Drubin DG (2013). Ultrastructural imaging of endocytic sites in Saccharomyces cerevisiae by transmission electron microscopy and immunolabeling. Microsc Microanal 19, 381–392.

Collins A, Warrington A, Taylor KA, Svitkina T (2011). Structural organization of the actin cytoskeleton at sites of clathrin-mediated endocytosis. Curr Biol 21, 1167–1175.

Galletta BJ, Chuang DY, Cooper JA (2008). Distinct roles for Arp2/3 regulators in actin assembly and endocytosis. PLoS Biol 6, e1.

Goode BL, Eskin JA, Wendland B (2015). Actin and endocytosis in budding yeast. Genetics 199, 315–358.

Huang F, Hartwich TM, Rivera-Molina FE, Lin Y, Duim WC, Long JJ, Uchil PD, Myers JR, Baird MA, Mothes W, *et al*. (2013). Video-rate nanoscopy using sCMOS camera-specific single-molecule localization algorithms. Nat Methods 10, 653–658.

Idrissi FZ, Grotsch H, Fernandez-Golbano IM, Presciatto-Baschong C, Riezman H, Geli MI (2008). Distinct acto/myosin-I structures associate with endocytic profiles at the plasma membrane. J Cell Biol 180, 1219–1232.

Kaksonen M, Toret CP, Drubin DG (2005). A modular design for the clathrin- and actin-mediated endocytosis machinery. Cell 123, 305–320.

Kukulski W, Schorb M, Kaksonen M, Briggs JA (2012). Plasma membrane reshaping during endocytosis is revealed by time-resolved electron tomography. Cell 150, 508–520.

Laplante C, Huang F, Bewersdorf J, Pollard TD (2016a). High-speed super-resolution imaging of live fission yeast cells. Methods Mol Biol 1369, 45–57.

Laplante C, Huang F, Tebbs IR, Bewersdorf J, Pollard TD (2016b). Molecular organization of cytokinesis nodes and contractile rings by super-resolution fluorescence microscopy of live fission yeast. Proc Natl Acad Sci USA 113, E5876–E5885.

Lee WL, Bezanilla M, Pollard TD (2000). Fission yeast myosin-I, Myo1p, stimulates actin assembly by Arp2/3 complex and shares functions with WASp. J Cell Biol 151, 789–800.

Lu R, Drubin DG, Sun Y (2016). Clathrin-mediated endocytosis in budding yeast at a glance. J Cell Sci 129, 1531–1536.

Minc N, Boudaoud A, Chang F (2009). Mechanical forces of fission yeast growth. Curr Biol 19, 1096–1101.

Padrick SB, Cheng HC, Ismail AM, Panchal SC, Doolittle LK, Kim S, Skehan BM, Umetani J, Brautigam CA, Leong JM, Rosen MK (2008). Hierarchical regulation of WASP/WAVE proteins. Mol Cell 32, 426–438.

Picco A, Mund M, Ries J, Nedelec F, Kaksonen M (2015). Visualizing the functional architecture of the endocytic machinery. Elife 4, doi:10.7554/eLife.04535.

Rajmohan R, Wong MH, Meng L, Munn AL, Thanabalu T (2009). Las17p-Vrp1p but not Las17p-Arp2/3 interaction is important for actin patch polarization in yeast. Biochim Biophys Acta 1793, 825–835.

Schaber J, Adrover MA, Eriksson E, Pelet S, Petelenz-Kurdziel E, Klein D, Posas F, Goksor M, Peter M, Hohmann S, Klipp E (2010). Biophysical properties of Saccharomyces cerevisiae and their relationship with HOG pathway activation. Eur Biophys J 39, 1547–1556.

Sirotkin V, Beltzner CC, Marchand JB, Pollard TD (2005). Interactions of WASp, myosin-I, and verprolin with Arp2/3 complex during actin patch assembly in fission yeast. J Cell Biol 170, 637–648.

Sirotkin V, Berro J, Macmillan K, Zhao L, Pollard TD (2010). Quantitative analysis of the mechanism of endocytic actin patch assembly and disassembly in fission yeast. Mol Biol Cell 21, 2894–2904.

Skruzny M, Brach T, Ciuffa R, Rybina S, Wachsmuth M, Kaksonen M (2012). Molecular basis for coupling the plasma membrane to the actin cytoskeleton during clathrin-mediated endocytosis. Proc Natl Acad Sci USA 109, E2533–E2542.

Sun Y, Leong NT, Jiang T, Tangara A, Darzacq X, Drubin DG (2017). Switch-like Arp2/3 activation upon WASP and WIP recruitment to an apparent threshold level by multivalent linker proteins in vivo. Elife 6, e29140.

Sun Y, Martin AC, Drubin DG (2006). Endocytic internalization in budding yeast requires coordinated actin nucleation and myosin motor activity. Dev Cell 11, 33–46.

Wang S, Moffitt JR, Dempsey GT, Xie XS, Zhuang X (2014). Characterization and development of photoactivatable fluorescent proteins for single-molecule-based superresolution imaging. Proc Natl Acad Sci USA 111, 8452–8457.

Young ME, Cooper JA, Bridgman PC (2004). Yeast actin patches are networks of branched actin filaments. J Cell Biol 166, 629–635.